THE JOURNAL OF PHYSICAL CHEMISTRY

Universitat d'Alacant
Universidad de Alicante

C: Plasmonics, Optical Materials, and Hard Matter

Density Functional Theory Modeling of Solid-State Nuclear Magnetic Resonances for Polycyclic Aromatic Hydrocarbons

Virginia Diez-Gómez, Isabel Sobrados, Jesús Sanz, Manuel Carrera, Albert Guijarro, Jose A Verges, and Pedro L de Andres

J. Phys. Chem. C, **Just Accepted Manuscript** • DOI: 10.1021/acs.jpcc.8b02340 • Publication Date (Web): 24 Apr 2018

ACS Publications

is published by the American Chemical Society. 1155 Sixteenth Street N.W., Washington, DC 20036

Density Functional Theory Modeling of Solid-State Nuclear Magnetic Resonances for Polycyclic Aromatic Hydrocarbons

Virginia Diez-Gomez,*,† Isabel Sobrados,† Jesus Sanz,† Manuel Carrera,‡ Albert Guijarro,‡ Jose A Verges† and Pedro L de Andres¶

†Instituto de Ciencia de Materiales de Madrid,
Consejo Superior de Investigaciones Cientificas, Madrid, Spain

‡Departamento de Química Orgánica and Instituto de Síntesis Orgánica,
Universidad de Alicante, Spain

¶ Instituto de Ciencia de Materiales de Madrid,
Consejo Superior de Investigaciones Cientificas, Madrid, Spain
and
Donostia International Physics Center, Donostia, Spain

E-mail: virginia.diez@icmm.csic.es

Abstract

Experimental Solid State Nuclear Magnetic Resonance (SS-NMR) has been used to analyze different theoretical models for Polycyclic Aromatic Hydrocarbon crystals of similar structure (naphthalene, anthracene, phenanthrene, picene, and triphenylene). We compare the accuracy of four modeling approaches to compute SS-NMR chemical shifts using ab-initio Density Functional Theory (DFT). Models based on X-Ray cell parameters, on optimization of cell with Perdew, Burke and Ernzerhof (PBE) approximation and on two methods adding dispersion forces were compared (using Pearson's and Mean Absolute Deviation correlation factors). Even if the intermolecular distances and cell volumes are different depending on the model, there is an overall good agreement between theoretical and experimental ^{13}C chemical shifts for all of them. An analysis of intermolecular distances and deviation from planarity in different models and their influence on theoretical chemical shieldings is also performed.

Introduction

Solid-State Nuclear Magnetic Resonance (SS-NMR) is a structural technique with a considerable sensitivity to the position of atomic nuclei (cores). Precise ways to compute NMR shifts through Density Functional Theory (DFT)[1-2] in finite-size clusters have been available for some time using the Gauge-Independent Atomic Orbital method (GIAO)[3], and more recently the Continuous Set of Gauge Transformations (CSGT)[4]. Computation of chemical shifts based on plane waves and DFT, which is best adapted to extended, periodic systems, has been developed in a direct[5-6] and a converse[7] approach. Over the last decade, the use of Gauge-Independent Projector Augmented Wave Pseudopotentials (GIPAW)[8-9] has demonstrated considerable success computing NMR resonances in extended systems[10]. The concept of NMR crystallography has emerged by the combined use of experimental NMR and diffraction data with theoretical results obtained by DFT. A book[11] and thematic issues[12-14] have been dedicated to this structural approach. The method involved in NMR crystallography and examples covering a wide variety of materials are reviewed by Martineau et al[15]. In particular this approach is used by Czernek et al.[16-17] to predict and assign SS-NMR spectra of organic systems and by Dudenko et al.[18] and Kobayashi et al.[19] to analyze intermolecular packing of organic materials.

In this context, this work has three goals. First, we seek to further our knowledge of crystals of polycyclic aromatic hydrocarbons (PAHs), which are molecules that attract attention for a number of different reasons, just to cite two of them, its potential role in hydrogen storage and in the chemistry of protoplanetary disks surrounding young stars[20-21]. NMR analyses for some of these (e.g. naphthalene and anthracene) have been previously reported in the literature[7, 22]. Second, we seek to compare solid-state NMR calculations for PAH crystals based on GIPAW, with the aim to further the experience on fundamental choices for the theory like the exchange and correlation functional, or the role of dispersion forces. We use quantitative R-factors to discriminate among models for NMR data. Following ideas that have been proved useful in other structural techniques (e.g. LEED or XRD), we argue that the best way to construct agreement R-factors is to make it dependent on positions of peaks only. Uncertainties related to peak widths, both theoretical and experimental, advise using R-factors as insensitive to them as possible. Finally, we analyze differences between methods in determining intermolecular distances and planarity of molecules which highlight the different approaches used to include dispersion forces. Their influence on certain chemical shieldings is also reported.

Experimental

Samples

PAHs samples of naphthalene (99%), anthracene (>99%), phenanthrene (>99.5%), and triphenylene (98%), were best grade commercially available (Sigma-Aldrich). Picene(>99%) was synthesized by a photochemical route and purified by recrystallization from toluene[23].

MAS-NMR

^{13}C CP-MAS NMR spectra were obtained in a Bruker Avance 400 spectrometer, using a standard cross-polarization pulse sequence. Samples were spun at 10 kHz in MAS (magic-angle-spinning) NMR experiments. Spectrometer frequencies were set at 100.62 and 400.13 MHz for ^{13}C and ^{1}H respectively. A contact time of 2 ms and a period between successive accumulations of 240 s were used. To improve resolution ^{13}C spectra were recorded during ^{1}H decoupling. The number of scans was 600. Chemical shift values were referenced to TMS. The NQS (Non-Quaternary Suppression) sequence has been used to identify the quaternary carbons.

Theory

NMR chemical shifts have been computed using plane-waves as implemented in CASTEP (v8.0)[24] and VASP (v5.4)[25]. The exchange and correlation functional has been approximated by the generalized gradient approximation due to Perdew, Burke and Ernzerhof (PBE)[26]. For plane-waves, we have used cutoff energies in the range of 775 to 725 eV corresponding to pseudopotentials implemented by Pickard et al.[8] (CASTEP) and PAW[27-28] (VASP), and k-points spacing grids of 0.4 nm^{-1}. These values ensured that chemical shifts were converged better than 1 ppm. Other threshold parameters for CASTEP/VASP are as follows: total energy converged to better than 10^{-7} eV, a maximum force on any atom better than 0.05 eV/nm, a maximum atom displacement of less than $5x10^{-5}$ nm, and a maximum stress on the unit cell better than 0.02 GPa. Semi-empirical dispersion corrections have been included following Tachenko and Scheffler[29] as implemented in the CASTEP code by McNellis, Meyer and Reuter[30]. The non-local functional proposed in the literature to include van der Waals interactions inside the self-consistency cycle[31-32] has been used as recommended by Soler et al.[31] in VASP.

Results and Discussion

We report SS-NMR experiments and DFT calculations on five PAHs: naphthalene ($C_{10}H_8$), anthracene ($C_{14}H_{10}$), phenanthrene ($C_{14}H_{10}$), picene ($C_{22}H_{14}$) and triphenylene ($C_{18}H_{12}$). The four first molecules are linear while the last one is disc-shaped. Naphthalene and anthracene belong to the acene family and phenanthrene and picene to the phenacene family. Assuming that all these molecules are planar and lie on a mirror plane, naphthalene and anthracene possess one binary axis perpendicular to that plane and two mirror planes resulting in three and four chemically inequivalent carbon atoms respectively. Phenanthrene and picene only possess an additional mirror plane, increasing the number of inequivalent carbon atoms to seven and eleven, respectively. In the case of triphenylene, there are three additional mirror planes and a ternary axis giving only three inequivalent carbon atoms. The four linear molecules crystallize in a monoclinic unit cell, naphthalene and anthracene belonging to space group num. 14 in the international tables for crystallography ($P2_1/c$), and phenanthrene and picene to space group num. 4 ($P2_1$). They present a stacking in sheets showing CH-π hydrogen bonds. Molecular stacking in these four compounds is similar to the one shown in Figure 4 for naphthalene. The interaction between molecules is weak, either due to electrostatic interaction of permanent dipoles with their images in neighboring electronic clouds (CH-π) or electrostatic

interaction of fluctuating dipoles (van der Waals). The fifth compound studied (triphenylene) crystallizes in space group num. 19 ($P2_12_12_1$). The stacking in this compound is built by CH-π and π-π interactions. In these molecules, internal C-C and C-H chemical bonds are well described as sp^2 hybridized orbitals, with C-C distances in the range 136-146 pm and C-H distances near 109 pm.

Fig.1 shows a schematic description of these molecules with the carbon atoms classified in five types: (1) tertiary at the short end (apex) of the molecule (green), (2) tertiary on the zigzag edges (blue), (3) tertiary at the armchair bay (purple), (4) quaternary on the zigzag edges (red) and (5) quaternary at the armchair bay (orange).

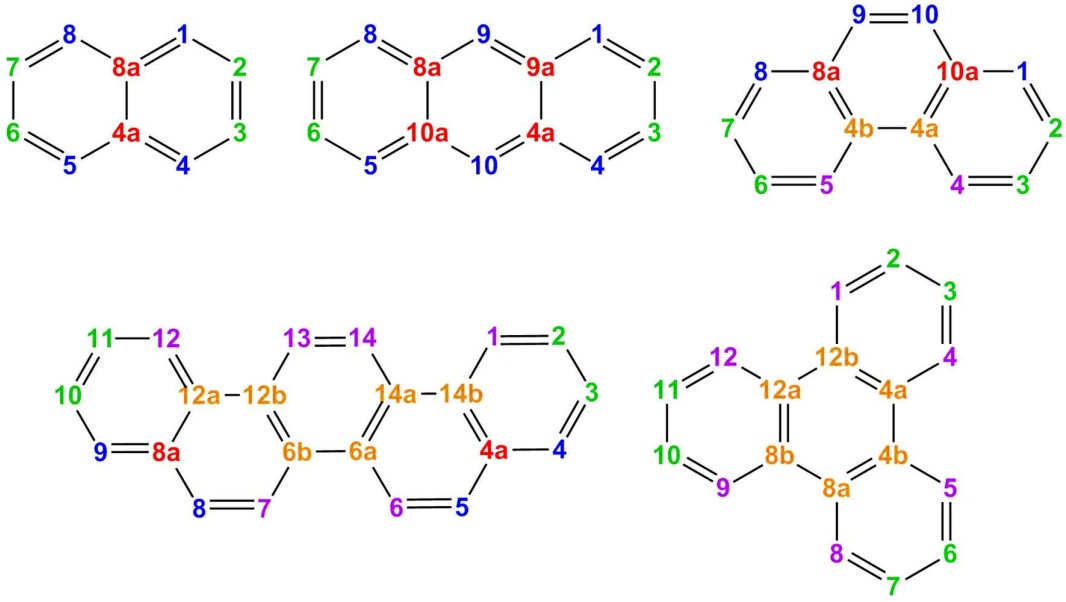

Figure 1. Schematic view of naphthalene ($C_{10}H_8$), anthracene ($C_{14}H_{10}$), phenanthrene ($C_{14}H_{10}$), picene ($C_{22}H_{14}$) and triphenylene ($C_{18}H_{12}$) molecules where different types of carbon atoms associated to different NMR shifts are denoted by the following color code (common to Table 1): green (apex), blue (tertiary zigzag), purple (tertiary armchair bay), red (quaternary zigzag) and orange (quaternary armchair bay).

NMR spectra

Spectra obtained in solution show the same number of resonances as predicted by theory for naphthalene, anthracene and triphenylene. For phenanthrene, NMR signals corresponding to carbons labelled two and seven overlap with those marked three and six. In the case of picene, all peaks have been resolved and are reported here for the first time. (Table 1 gives the detailed chemical shift values)

The crystal packing of these compounds reduces the symmetry in the molecules, thus increasing the number of independent peaks. While naphthalene and anthracene keep an inversion center, all carbon atoms become inequivalent for phenanthrene, picene and triphenylene. Therefore, the number of solid-state NMR resonances increase theoretically up to 5, 7, 14, 22 and 18, respectively, but not all peaks could be resolved in powder samples.

The solid-state NMR spectra (Figure 2) were best-fitted with Gaussians or mixed Gaussian/Lorentzians. Chemical shifts of deconvoluted peaks are summarized in Table 1. Regarding line widths, we argue that a precise knowledge of their values is not crucial to retrieve useful information; they depend on different experimental factors that are difficult to control and are also difficult to compute from theoretical models. Typical values for linewidths in triphenylene (best case) as determined from fitted normalized Lorentzian functions are between 0.1 and 1 ppm.

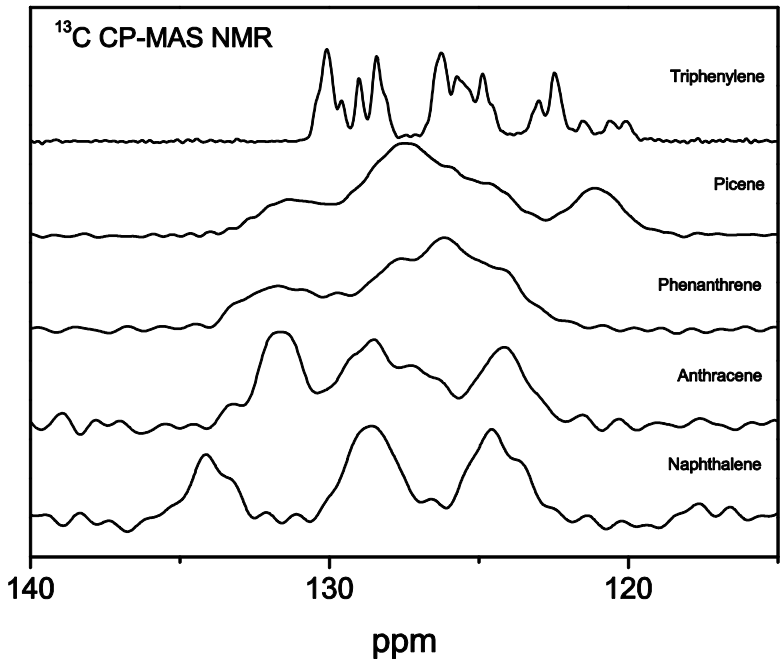

Figure 2. Experimental ^{13}C CP-MAS NMR spectra for triphenylene, picene, phenanthrene, anthracene and naphthalene.

Experimental resolution in naphthalene and anthracene ^{13}C CP-MAS NMR spectra allows the identification of the same number of peaks as in solution: three and four peaks respectively. For phenanthrene, we have obtained a deconvolution composed of seven not well-resolved peaks; two are detected at 132.22 and 130.31 ppm (quaternary carbons) and another five are between 128.46 and 122.59 ppm (one more than in solution). Picene also presents a not well-resolved spectrum with eight components (one more than in solution) that reproduce well the experimental profile. Thus the number of peaks for the first four compounds correlates to the number of inequivalent atoms in isolated molecules.

On the other hand, triphenylene shows twelve well-resolved peaks (labelled from 1 to 12 in graphical TOC), and six shoulders (A to F), which correspond to the 18 expected resonances, grouped in three sets of six elements. In the case of triphenylene, the small width of the components suggests the presence of residual molecular precessions around a ternary axis, which reduces dipolar H-H interactions, improving the spectral resolution of its components.

The assignment of NMR peaks to different carbon atoms was performed according to DFT calculations. Differences between solid state and solution NMR chemical shifts are

below 1.5 ppm in acene compounds but can go up to 3.2 ppm in the case of triphenylene, e.g. see Table 1.

Table 1. (Color online). ^{13}C NMR shifts for the different samples considered in the paper: (1) Experimental values for dissolution ("exp. dissol."), (2) Experimental values for solid-state ("exp. sol."), (3) Theoretical values for solid-state ("calc. sol."), (4) Fractional contribution of each adjusted peak to the experimental NMR spectra (solid-state). The color code corresponds to Figure 1: red (quaternary zigzag), orange (quaternary armchair bay), blue (tertiary zigzag), green (apex), and purple (tertiary armchair bay).

	quaternary zigzag	quaternary armchair bay	tertiary zigzag	apex	tertiary armchair bay
NAPHTHALENE	4a, 8a		1, 5, 4, 8	3, 7, 2, 6	
exp. dissol.	133.45		127.84	125.75	
exp. sol.	134.1		128.6	124.6	
calc. sol.	135.1		128.5; 128.1	124.7;123.8	
area %	20.57		41.13	38.30	
ANTHRACENE	9a, 10a, 4a, 8a		4, 8, 1, 5	9, 10	2, 6, 3, 7
exp. dissol.	131.70		128.16	126.21	125.33
exp. sol.	131.7		128.7	126.8	124.2
calc. sol.	132.6; 132.2		128.7; 128.6	126.4	124.4; 124.3
area %	28.92		30.99	13.26	26.82

PHENANTHRENE	10a, 4a	8a, 4b	9, 8	1, 3	7, 10	2, 5	6, 4
exp. dissol.	131.99	130.25	126.84;128.46	128.46; 126.46	126.84; 126.46	126.46; 122.59	126.46;122.59
exp. sol.	132.3	130.6	128.6	127.5	126.2	125.0	123.8
calc. sol.	134.0; 132.5	132.4; 130.2	128.1; 127.9	127.2; 125.7	125.6; 125.5	125.4; 123.9	122.9; 122.7
area %	14.00	11.97	13.27	14.50	16.85	15.68	13.74

PICENE	4a, 14b	8a, 12a	6b, 12b	6a, 14a, 9, 8, 4	2, 10, 5, 3	12, 1, 11	6, 14, 7, 13
exp. dissol.	132.02;130.58	132.02; 130.58	128.68; 128.69	128.68;128.69; 128.56; 127.56; 128.56	126.84; 126.62; 127.56; 126.62	123.17; 123.17; 126.84	121.70;121.67; 121.70; 121.67
exp. sol.	131.9	130.8	128.9	127.5	125.9	124.3	121.1
calc. sol.	133.0;132.4	132.1;130.4	130.2; 128.8	128.7- 127:0	125.7-125.3	124.1-122.8	121.2-119.5
area %	7.15	8.41	11.25	26.50	16.30	13.50	17.06

TRIPHENYLENE	12a	8a	4a	8b	12b	C4b	7	11	6	3	2	10	9	8	5	12	4	1
exp. dissol.	129.82	129.82	129.82	129.82	129.82	129.82	127.21	127.21	127.21	127.21	127.21	127.21	123.31	123.31	123.31	123.31	123.31	123.31
exp. sol.	130.4	130.1	129.6	129.0	128.5	128.2	126.5	126.2	125.7	125.4	124.9	124.5	123.1	122.5	122.5	121.5	120.6	120.1
calc. sol.	131.7	131.5	130.9	130.8	130.7	130.6	126.6	126.1	125.3	125.3	124.7	124.2	123.3	122.5	121.3	120.8	120.3	118.9
area %	3.50	12.12	2.61	6.06	7.59	5.12	6.88	8.75	7.18	5.51	8.15	2.73	6.10	9.57	9.57	2.73	2.71	2.68

DFT calculations

The starting point for the crystal structures of the different compounds was the X-rays structural determination as found in the literature[32-36]. DFT was then used at different levels of sophistication to optimize the geometry of the cell and the positions of the atoms forming its basis.

We compare four different approaches to calculate solid-state NMR resonances: (1) optimization of the atomic positions of H and C atoms inside the unit cell, while keeping fixed the experimental XRD parameters for the unit cell (XRD), (2) optimization of forces on every atom and stresses on the periodic cell, using for exchange and correlation the PBE approximation (PBE), (3) same procedure than the previous one but adding semi-empirical dispersion corrections (VDW1) and (4) adding ab-initio dispersion corrections (VDW2).

After geometry optimization by XRD, PBE and VDW1 methods, bond distances differ less than 0.6 pm. We notice that DFT calculations validate Clar's aromatic π-sextet rule which states that the aromatic character of benzenoid species could be used to predict shorter or longer C-C distances in the molecules of this study. In the compounds of Figure 1 the shorter bonds are the ones linking either blue carbon atoms with each other, or blue and purple carbon atoms, indicating a high double bond character. On the other hand, the longest distances are the ones linking orange carbon atoms labelled with the same number, evidencing a high single bond character.

Intermolecular distances are more clearly influenced by the method used in geometry optimization. The shorter intermolecular distance in each compound calculated by PBE method is 30-60 pm longer than calculated by the other three methods. While the same distance calculated by XRD, VDW1 and VDW2 differ less than 15 pm. This is caused by the constraints (XRD) or the different description of intermolecular interactions (PBE, VDW1 and VDW2). Intermolecular interactions are mostly responsible for the shape and size of the periodic cell. In Table 2 cell parameters of the five compounds of this study optimized by the four methods described above are summarized. It is shown the well-known inadequacy of PBE to describe interactions where correlation dominates, as are the van der Waals, CH-π hydrogen bond or image forces. The unit cell volumes are overestimated with this method by as much as 35%. VDW1 causes a decrease of cell volume between 3 and 5% and VDW2 modifies it in less than 2%.

The order of carbon atoms arranged by increasing chemical shielding showed slight differences in the sequences among the different methods in phenanthrene, picene and triphenylene. As VDW2 showed the best Pearson's correlation factor between theoretical and experimental chemical shifts for naphthalene and anthracene and its cell volume was also the closest to the experimental one, the assignment of increasing experimental chemical shift to increasing calculated chemical shieldings was done according to this method.

Table 2: Structural data for unit cells (left): Lengths a, b, c (in pm). Angles α, β, γ (in °). Volume V (in nm^3) and merit factor (right): Mean absolute deviation for NMR shifts, $D = \frac{1}{N}\sum_{i=1}^{N}|e_i - t_i|$(in ppm)

	a (pm)	b (pm)	c (pm)	α (°)	β (°)	γ (°)	V (nm^3)	D (ppm)
Naphthalene								
XRD[32]	794	595	817	90	115.10	90	0.350	0.87
PBE	869	648	923	90	119.05	90	0.455	0.39
VDW1	786	587	807	90	114.43	90	0.339	0.87
VDW2	804	594	817	90	116.42	90	0.349	0.49
Anthracene								
XRD[33]	855	602	1117	90	124.60	90	0.473	1.04
PBE	974	656	1171	90	123.83	90	0.621	0.61
VDW1	836	594	1107	90	125.07	90	0.450	1.02
VDW2	852	597	1104	90	123.93	90	0.465	0.31
Phenanthrene								
XRD[34]	844	614	944	90	97.96	90	0.484	0.86
PBE	971	652	981	90	100.40	90	0.611	1.12
VDW1	849	583	933	90	97.51	90	0.458	0.98
VDW2	848	605	932	90	97.84	90	0.474	0.86
Picene								
XRD[35]	848	615	1352	90	90.46	90	0.705	0.62
PBE	978	652	1389	90	92.45	90	0.884	0.87
VDW1	856	584	1342	90	90.15	90	0.671	0.76
VDW2	853	609	1341	90	90.32	90	0.696	0.85
Triphenylene								
XRD[36]	1297	1670	528	90	90	90	1.144	0.99
PBE	1469	1521	695	90	90	90	1.552	0.96
VDW1	1298	1645	514	90	90	90	1.098	1.23
VDW2	1315	1663	524	90	90	90	1.146	0.81

To evaluate quantitatively the validity of the four methods, correlations between computed chemical shieldings (σ) vs the measured chemical shifts (δ) were calculated (shown in Figure 3). Since the latter are referred to an arbitrary common origin (TMS), it is first necessary to determine a value for the offset between theory and experiment. This is accomplished by a least squares fit to the equation $\delta = \sigma_0 - m \cdot \sigma$. Although ideally m should be equal to one, it is frequently observed a small deviation from this value[37-39]. As the range of chemical shifts involved in this work is small, the effect of a slope close to one will be weak. Using different slopes for each method could disturb a direct

comparison between different theoretical approaches. For these reasons, we have decided to consider m=1 in all cases.

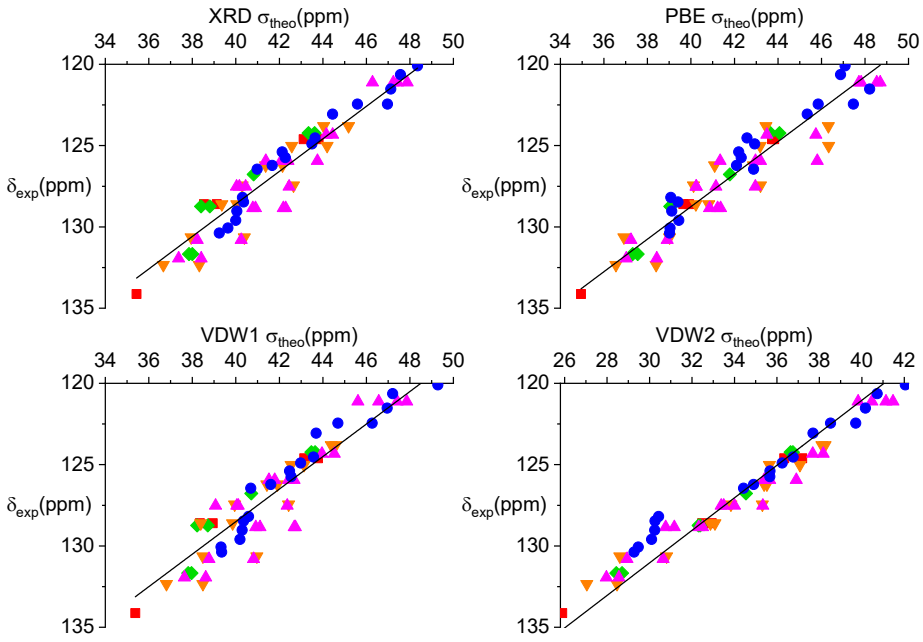

Figure 3. For the entire database, determination of a common offset between theoretical chemical shieldings (σ) and experimental chemical shifts (δ) from a least-squares fit of the form $\delta = \sigma_0 - \sigma$. Values for σ_0 are 168.6 ppm for XRD (upper left panel), 168.8 ppm for PBE (upper right panel), 168.5 for VDW1 (lower left panel) and 161.0 ppm for VDW2 (lower right panel). The database is composed of: (1) red squares: naphthalene, (2) green diamonds: anthracene, (3) orange down triangles: phenanthrene, (4) magenta up triangles: picene, (5) blue circles: triphenylene.

We obtain the following values for σ_0: 168.6 ± 0.3, 168.8 ± 0.3 ,168.5 ± 0.3 and 161.0 ± 0.2 ppm, respectively for XRD, PBE, VDW1 and VDW2 models. Pearson's correlation coefficients (a measure of the linear correlation between variables δ and σ) computed for each method according to the assignment of VDW2 method are: 0.949, 0.952, 0.931 and 0.961, while the mean absolute residual errors (a measure of the dispersion of data around the fitted straight line) are 0.88, 0.83, 0.99 and 0.70 ppm, respectively for XRD, PBE, VDW1 and VDW2. We remark that the mean absolute error is good for all models, always below 1 ppm considering all the compounds of this study. In Table 2 (right) the mean absolute deviation obtained for each compound with each theoretical model is shown. We can observe that there is not one model with the smaller mean deviation for all the compounds and all mean deviations are smaller than 1.25 ppm showing the accuracy of all the tested methods. Table 1 compares detailed values for the experimental chemical shifts and the theoretical results with VDW2 approach; we have used five different colors to highlight that each type of carbon belongs to a characteristic range of chemical shifts values.

As commented above, we expect solid-state NMR technique to be more sensitive to the atomic positions determined by the intramolecular electronic structure, and less sensitive to the intermolecular interactions that determine the size and shape of the unit cell. Holmes et al.[40] investigated the intermolecular effects on ^{13}C NMR chemical-shielding

tensors modeling organic systems as isolated molecules and molecular clusters. A study of intermolecular effects under periodic boundary conditions could be done comparing the calculation of the crystal with that of a molecule in a cell surrounded of enough vacuum to consider it isolated from the molecules of neighboring unit cells[41]. Instead of that, we have considered that certain effects of packing could be detected directly on crystals and its influence on chemical shielding studied. One of this effects is the bending or deviation from planarity and another one is the differentiation of atoms that would be equivalent in solution. Following these ideas, we have analyzed the deviation from planarity of the molecules in the different systems. In the crystal structures obtained by XRD, the mean deviation of C atoms from the best fit plane of the molecule is always smaller than 3.5 pm. In the DFT geometry optimized models we have found that naphthalene and anthracene (lineal molecules which keep an inversion center in the crystal) showed a mean deviation smaller than 5 pm. And the difference between the chemical shielding of carbon atoms that would be equivalent in solution is smaller than 0.7 ppm. For phenanthrene and picene the mean deviation of the model calculated by PBE method is around 10 pm, having also a difference in chemical shielding (of C atoms equivalent in solution) smaller than 0.7 ppm. However, for phenanthrene and picene with XRD, VDW1 and VDW2 methods and for triphenylene (with all the methods) the mean deviation is always bigger than 15 pm. All those models show at least a couple of carbon atoms that are equivalent in solution whose chemical shieldings differ more than 1.5 ppm (in one case as much as 5.6 ppm) in calculations performed on the crystals. In this way it is stated that the deviation from planarity caused by packing can have a considerable influence on chemical shieldings of carbon atoms in these molecules.

In the case of naphthalene (which do not deviate significantly from planarity) C1, C4, C5 and C8 are equivalent in solution, but the calculated shielding for C1 (and C5 which is equivalent in the crystal structure) is lower than for C4 (and C8). If we take a closer look at the structure (Figure 4) we can see that C1 and C5 are the ones involved in CH-π interaction with neighboring molecules. DFT calculations with all methods assign less shielding to those carbon atoms compared to their homologues which are more distant to the nearest molecule. The difference in shielding is smaller for PBE method (0.27 ppm), bigger for VDW2 (0.46 ppm) and even bigger for XRD and VDW1 (0.59 ppm). These differences correlate with decreasing distances between the H atom and the center of the neighboring ring. The effect on the shielding of H atoms involved in CH- π interaction is greater. H1 is 1.95, 2.79, 2.88 or 3.08 ppm more shielded than H4 depending on the method used: PBE, XRD, VDW1 or VDW2. Due to the difficulty in obtaining a resolved ^{1}H spectrum of this compound we could not corroborate experimentally this prediction. In anthracene, the intermolecular distances are not so different comparing carbon or hydrogen atoms which are equivalent in solution and we could not find such a clear influence between packing and chemical shielding.

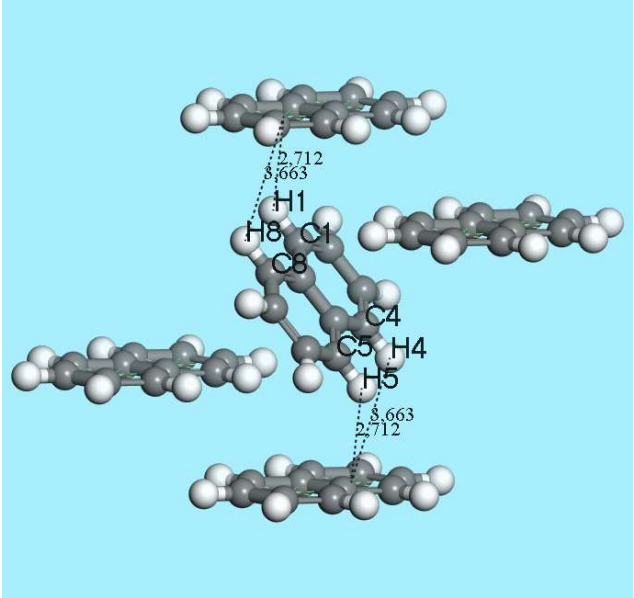

Figure 4 Intermolecular distances between H atoms and the center of the nearest aromatic ring in the model obtained for naphthalene with VDW2 method.

CONCLUSIONS

Often, the inherent insolubility and poor crystallinity of large-sized PAHs represent an insurmountable obstacle for an adequate structural characterization. While reasons that affect the experimental resolution of solid state ^{13}C CP-MAS NMR are not easily attributed to well-defined variables, badly resolved spectra of solid polycyclic aromatic hydrocarbons can be analyzed with the help of methods investigated in this work. It is observed that homologous series of PAHs belonging to the same family (e.g. acenes, phenacenes, p-phenyls, etc.) tend to pack in similar crystal structures, often within the same space group. In addition, they tend to display a linear correlation between the length of the cell axes and the length of the molecular axes as the molecular size increases within the series[42]. Extrapolation from the internal crystalline structure of known crystals of small PAHs towards their larger problematic homologues is a simple exercise, setting the initial seeds for plane-waves DFT optimization and solid state NMR analysis. We expect that the procedures described here will help experimentalists in the task of structural characterization of high molecular weight PAHs, such as graphene segments, nanoribbons and islands, for which few techniques of experimental elucidation are available when dealing with the bulk.

The combined use of Pearson's correlation coefficient, and the mean absolute deviation from experiment and theory shows that calculations based on ab-initio dispersion corrections (VDW2) yield a nice agreement in both the structural parameters and the NMR chemical shifts, with an averaged mean absolute deviation over all the compounds of <D>= 0.70 ppm. On the other hand, PBE yields a consistent agreement with the positions of the resonances, with <D>= 0.83 ppm, but cannot reproduce well the size and shape of the unit cell for these materials. PBE tends to overestimate the distances between molecules due to its limited amount of correlation. Including dispersion forces via a semi-empirical scheme improves these distances and restores volumes for the unit cell to

similar values than determined by XRD. Bonding distances between pairs of C-C and C-H get values that agree well with reported values in the literature, independently of the different approximations. Typical C-C distances within the family of PAHs show roughly three peaks: around 136 to 138 pm for the lowest, 139 to 142 pm for the intermediate, and 143 to 146 pm for the largest one. We should comment in passing that models based in a local density approximation for exchange and correlation consistently produced worse results.

SS-NMR chemical shifts are sensitive to feel some effects of packing. DFT calculations predict two main effects. Mean deviations of carbon atoms, from the best fit plane of those molecules, higher than 15 pm cause differences in chemical shieldings higher than 1.5 ppm in some of the carbon atoms that are equivalent in solution. In naphthalene, the effects of CH-π interaction on chemical shieldings could be analyzed. We have seen that a decrease in the distance between the hydrogen atom and the ring of a neighboring molecule produces a significant increase in the chemical shielding of the hydrogen atom and some decrease in the chemical shielding of the carbon atom.

Acknowledgement

We are indebted to Dr. Maria Blanco-Rey for insightful comments on the role of different van der Waals functionals in DFT. We acknowledge funding from C. Madrid (Grant S2013/MIT-2753), MINECO (Grants MAT2014-54231, MAT2016-78625-C2-2P, and FIS2015-6422-C2-1-P), EU (Grant ERC-2013-SYG-610256 NANOCOSMOS), Generalitat Valenciana (Grant PROMETEO/2017/139), the University of Alicante, and computing resources from CTI-CSIC.

References

1. Hohenberg, P.; Kohn, W., Inhomogeneous electron gas. *Phys. Rev. B* **1964,** *136* (3B), B864-B871.

2. Kohn, W.; Sham, L. J., Self-consistent equations including exchange and correlation effects. *Physical Review* **1965,** *140*, A1133-A1138.

3. Wolinski, K.; Hinton, J. F.; Pulay, P., Efficient implementation of the gauge-independent atomic orbital method for NMR chemical-shift calculations. *J. Am. Chem. Soc.* **1990,** *112* (23), 8251-8260.

4. Keith, T. A.; Bader, R. F. W., Calculation of magnetic response properties using a continuous set of gauge transformations. *Chem. Phys. Lett.* **1993,** *210* (1-3), 223-231.

5. Mauri, F.; Pfrommer, B. G.; Louie, S. G., Ab initio theory of NMR chemical shifts in solids and liquids. *Phys. Rev. Lett.* **1996,** *77* (26), 5300-5303.

6. Sebastiani, D.; Parrinello, M., A new ab-initio approach for NMR chemical shifts in periodic systems. *J. Phys. Chem. A* **2001,** *105* (10), 1951-1958.

7. Thonhauser, T.; Ceresoli, D.; Marzari, N., NMR Shifts for Polycyclic Aromatic Hydrocarbons From First-Principles. *Int. J. Quantum Chem.* **2009,** *109* (14), 3336-3342.

8. Pickard, C. J.; Mauri, F., All-electron magnetic response with pseudopotentials: NMR chemical shifts. *Phys. Rev. B* **2001,** *63* (24), 13.

9. Yates, J. R.; Pickard, C. J.; Mauri, F., Calculation of NMR chemical shifts for extended systems using ultrasoft pseudopotentials. *Phys. Rev. B* **2007,** *76* (2), 11.

10. Bonhomme, C.; Gervais, C.; Babonneau, F.; Coelho, C.; Pourpoint, F.; Azais, T.; Ashbrook, S. E.; Griffin, J. M.; Yates, J. R.; Mauri, F.; Pickard, C. J., First-Principles Calculation of NMR Parameters Using the Gauge Including Projector Augmented Wave Method: A Chemist's Point of View. *Chem. Rev.* **2012,** *112* (11), 5733-5779.

11. Harris, R. K.; Wasylishen, R. E.; Duer, M. J., *NMR Crystallography*. Wiley: Chichester, U.K., 2009; p 520.

12. *Solid State Sciences* **2004,** *6* (10), 1019-1180.

13. *Crystengcomm* **2013,** *15* (43), 8589-8850.

14. *Solid State Nucl. Magn. Reson.* **2015,** *65*, 1-132.

15. Martineau, C.; Senker, J.; Taulelle, F., NMR Crystallography. In *Annual Reports on Nmr Spectroscopy, Vol 82*, Webb, G. A., Ed. 2014; Vol. 82, pp 1-57.

16. Czernek, J.; Brus, J., Theoretical predictions of the two-dimensional solid-state NMR spectra: A case study of the C-13-H-1 correlations in metergoline. *Chem. Phys. Lett.* **2013,** *586*, 56-60.

17. Czernek, J.; Brus, J., The covariance of the differences between experimental and theoretical chemical shifts as an aid for assigning two-dimensional heteronuclear correlation solid-state NMR spectra. *Chem. Phys. Lett.* **2014,** *608*, 334-339.

18. Dudenko, D. V.; Yates, J. R.; Harris, K. D. M.; Brown, S. P., An NMR crystallography DFT-D approach to analyse the role of intermolecular hydrogen bonding and pi-pi interactions in driving cocrystallisation of indomethacin and nicotinamide. *Crystengcomm* **2013,** *15* (43), 8797-8807.

19. Kobayashi, T.; Mao, K.; Paluch, P.; Nowak-Krol, A.; Sniechowska, J.; Nishiyama, Y.; Gryko, D. T.; Potrzebowski, M. J.; Pruski, M., Study of Intermolecular Interactions in the Corrole Matrix by Solid-State NMR under 100 kHz MAS and Theoretical Calculations. *Angew. Chem.-Int. Edit.* **2013,** *52* (52), 14108-14111.

20. Joblin, C.; Cernicharo, J., Detecting the building blocks of aromatics. *Science* **2018,** *359* (6372), 156-157.

21. Skov, A. L.; Thrower, J. D.; Hornekaer, L., Polycyclic aromatic hydrocarbons - catalysts for molecular hydrogen formation. *Faraday Discuss.* **2014,** *168*, 223-234.

22. Facelli, J. C.; Grant, D. M., DETERMINATION OF MOLECULAR SYMMETRY IN CRYSTALLINE NAPHTHALENE USING SOLID-STATE NMR. *Nature* **1993,** *365* (6444), 325-327.

23. Carrera, M.; de la Viuda, M.; Guijarro, A., 3,3 ',5,5 '-Tetra-tert-butyl-4,4 '-diphenoquinone (DPQ)-Air as a New Organic Photocatalytic System: Use in the Oxidative Photocyclization of Stilbenes to Phenacenes. *Synlett* **2016,** *27* (20), 2783-2787.

24. Clark, S. J.; Segall, M. D.; Pickard, C. J.; Hasnip, P. J.; Probert, M. J.; Refson, K.; Payne, M. C., First principles methods using CASTEP. *Zeitschrift Fur Kristallographie* **2005,** *220* (5-6), 567-570.

25. Kresse, G.; Marsman, M.; Furthmüller, J. *Vienna ab-initio package simulation*.

26. Perdew, J. P.; Burke, K.; Ernzerhof, M., Generalized gradient approximation made simple. *Physical Review Letters* **1996,** *77* (18), 3865-3868.

27. Blochl, P. E., Projector augmented-wave method. *Phys. Rev. B* **1994,** *50* (24), 17953-17979.

28. Kresse, G.; Joubert, D., From ultrasoft pseudopotentials to the projector augmented-wave method. *Phys. Rev. B* **1999,** *59* (3), 1758-1775.

29. Tkatchenko, A.; Scheffler, M., Accurate Molecular Van Der Waals Interactions from Ground-State Electron Density and Free-Atom Reference Data. *Phys. Rev. Lett.* **2009,** *102* (7), 4.

30. McNellis, E. R.; Meyer, J.; Reuter, K., Azobenzene at coinage metal surfaces: Role of dispersive van der Waals interactions. *Phys. Rev. B* **2009,** *80* (20), 10.

31. Roman-Perez, G.; Soler, J. M., Efficient Implementation of a van der Waals Density Functional: Application to Double-Wall Carbon Nanotubes. *Phys. Rev. Lett.* **2009,** *103* (9), 4.

32. Oddershede, J.; Larsen, S., Charge density study of naphthalene based on X-ray diffraction data at four different temperatures and theoretical calculations. *J. Phys. Chem. A* **2004,** *108* (6), 1057-1063.

33. Brock, C. P.; Dunitz, J. D., Temperature-dependence of thermal motion in crystalline anthracene. *Acta Crystallogr. Sect. B-Struct. Commun.* **1990,** *46*, 795-806.

34. Petricek, V.; Cisarova, I.; Hummel, L.; Kroupa, J.; Brezina, B., Orientational disorder in phenanthrene. Structure determination at 248, 295, 339 and 344 K. *Acta Crystallogr. Sect. B-Struct. Commun.* **1990,** *46*, 830-832.

35. De, A.; Ghosh, R.; Roychowdhury, S.; Roychowdhury, P., Structural-analysis of picene, C22H14. *Acta Crystallogr. Sect. C-Cryst. Struct. Commun.* **1985,** *41* (JUN), 907-909.

36. Ahmed, F. R.; Trotter, J., The crystal structure of triphenylene. *Acta Crystallographica* **1963,** *16* (6), 503-508.

37. Dumez, J.-N.; Pickard, C. J., Calculation of NMR chemical shifts in organic solids: Accounting for motional effects. *The Journal of Chemical Physics* **2009,** *130* (10), 104701.

38. Harris, R. K.; Hodgkinson, P.; Pickard, C. J.; Yates, J. R.; Zorin, V., Chemical shift computations on a crystallographic basis: some reflections and comments. *Magnetic Resonance in Chemistry* **2007,** *45*, S174-S186.

39. Webber, A. L.; Emsley, L.; Claramunt, R. M.; Brown, S. P., NMR Crystallography of Campho 2,3-c pyrazole (Z '=6): Combining High-Resolution H-1-C-13 Solid-State MAS NMR Spectroscopy and GIPAW Chemical-Shift Calculations. *J. Phys. Chem. A* **2010,** *114* (38), 10435-10442.

40. Holmes, S. T.; Iuliucci, R. J.; Mueller, K. T.; Dybowski, C., Density functional investigation of intermolecular effects on 13C NMR chemical-shielding tensors modeled with molecular clusters. *The Journal of Chemical Physics* **2014,** *141* (16), 164121.

41. Zilka, M.; Sturniolo, S.; Brown, S. P.; Yates, J. R., Visualising crystal packing interactions in solid-state NMR: Concepts and applications. *The Journal of Chemical Physics* **2017,** *147* (14), 144203.

42. Guijarro, A.; Verges, J. A.; San-Fabian, E.; Chiappe, G.; Louis, E., Herringbone Pattern and CH-pi Bonding in the Crystal Architecture of Linear Polycyclic Aromatic Hydrocarbons. *ChemPhysChem* **2016,** *17* (21), 3548-3557.

Graphical TOC